Journal of Marine Research, 53, 865–895, 1995

Journal of
MARINE RESEARCH

Volume 53, Number 6

Lateral mixing of the Mediterranean Water in the eastern North Atlantic

by M. Arhan[1] and B. King[2]

ABSTRACT

Analysis of the salinity distribution along three quasi-meridional hydrographic sections in the eastern North Atlantic shows that different mesoscale processes act to mix the Mediterranean Water with the adjacent water masses. In the region of transition with the Antarctic Intermediate Water in the south, the salt transport by the meddies seems to account for most of the observed lateral diffusive exchanges at the large scale. In the north these exchanges are contributed to by parcels of both Mediterranean Water and Subarctic Intermediate Water travelling on average in opposite directions. Also in the north but at a deeper level, transition with the Labrador Sea Water is characterized by a pronounced thermohaline front. Coherent mesoscale structures carrying deep Mediterranean Water escape northward from that front. A simplified unidirectional mixing model is used diagnostically to relate the basic parameters associated with the mesoscale structures to those characterizing lateral mixing at the large scale.

1. Introduction

The basin-wide salinity anomaly associated with the intrusion of Mediterranean Water (hereafter MW) in the North Atlantic is well suited to the quantification of the mixing of oceanic properties. Oceanographers indeed have not failed to take advantage of that well-defined thermohaline signal and, only considering lateral mixing, largely used it to infer estimates of both the large-scale and mesoscale diffusion coefficients.

1. Laboratoire de Physique des Océans, (CNRS-IFREMER-Université), IFREMER, Brest, B.P. 70, 29280 Plouzané, France.
2. Institute of Oceanographic Sciences, Wormley, Godalming, Surrey, GU8 5UB, United Kingdom.

At the large scale, Needler and Heath (1975) studied the balance between a mean westward advection of MW and three-dimensional diffusion. Using geostrophic estimates of the horizontal velocity they obtained large-scale diffusivities K_L ranging between 1.5 10^3 and 3 10^3 m^2 s^{-1}. Richardson and Mooney (1975) showed through numerical modelling that the shape of the Mediterranean salinity anomaly is compatible with the classical circulation pattern of the subtropical gyre, provided that the Peclet number[3] is in the range 3 to 30 or equivalently the large scale diffusivity between $\simeq$ 6 10^2 m^2 s^{-1} and $\simeq$ 5.5 10^3 m^2 s^{-1}.

On the southern flank of the Mediterranean intrusion in the so-called β-triangle, Armi and Stommel (1983) computed further estimates around $K_L \simeq 5\ 10^2\ m^2\ s^{-1}$ from the horizontal steady advective diffusive balance and tracer data from four cruises. Such typical values were confirmed in the same region by Hogg (1987) and on the northern flank of the tongue (47N, 15W) by Colin de Verdière *et al.* (1986).

The tracer fluxes associated with these large-scale diffusivities are the integrated result of mixing mechanisms occurring at the mesoscale. On the southern side, Armi *et al.* (1989) described the decay of an eddy carrying concentrated MW (meddy) which they followed during two years of its southward propagation. Hebert *et al.* (1990) showed that the rate of salt and heat loss in the same eddy was characterized by a horizontal diffusivity $K_M \simeq 5\ m^2\ s^{-1}$ which Joyce (1977) had shown to be associated with the interleaving phenomenon across sharp fronts. On the northern side, Colin de Verdière *et al.* (1986) showed how thermocline-intensified eddies could stir and mix the larger-scale salinity gradient of the MW below. Several approaches led these authors to estimates of the associated mesoscale diffusivities around $K_M \simeq 100\ m^2\ s^{-1}$.

The large-scale and mesoscale aspects have generally been addressed separately in the previous studies, and the links between the mixing parameters relative to both scales are not yet clearly established. Although the above diffusivities are still very uncertain, their orders of magnitude should now be considered sufficiently correct to justify a tentative effort to relate them together. This is the purpose of the present paper.

Our approach is mainly diagnostic: a simplified one-dimensional mixing model is used to reproduce the observed gradients on each side of the Mediterranean salinity maximum in the North-East Atlantic. Section 2 first describes the transition between the MW and the less saline adjacent water masses to the north and south, on the basis of three quasi-meridional hydrographic sections. The model linking the mixing parameters at the two scales is presented in Section 3 and used in the following to successively reproduce: (i) The transition with the Antarctic Intermediate Water (AAIW) in the south and the role of meddies as southward conveyors of Mediterra-

3. The Peclet number, a measure of the relative effects of advection to diffusion, is defined as $P_e = UL/K_L$, where U, L and K_L are typical values of, respectively, the large-scale velocity, the tracer anomaly length scale, and the large-scale diffusivity.

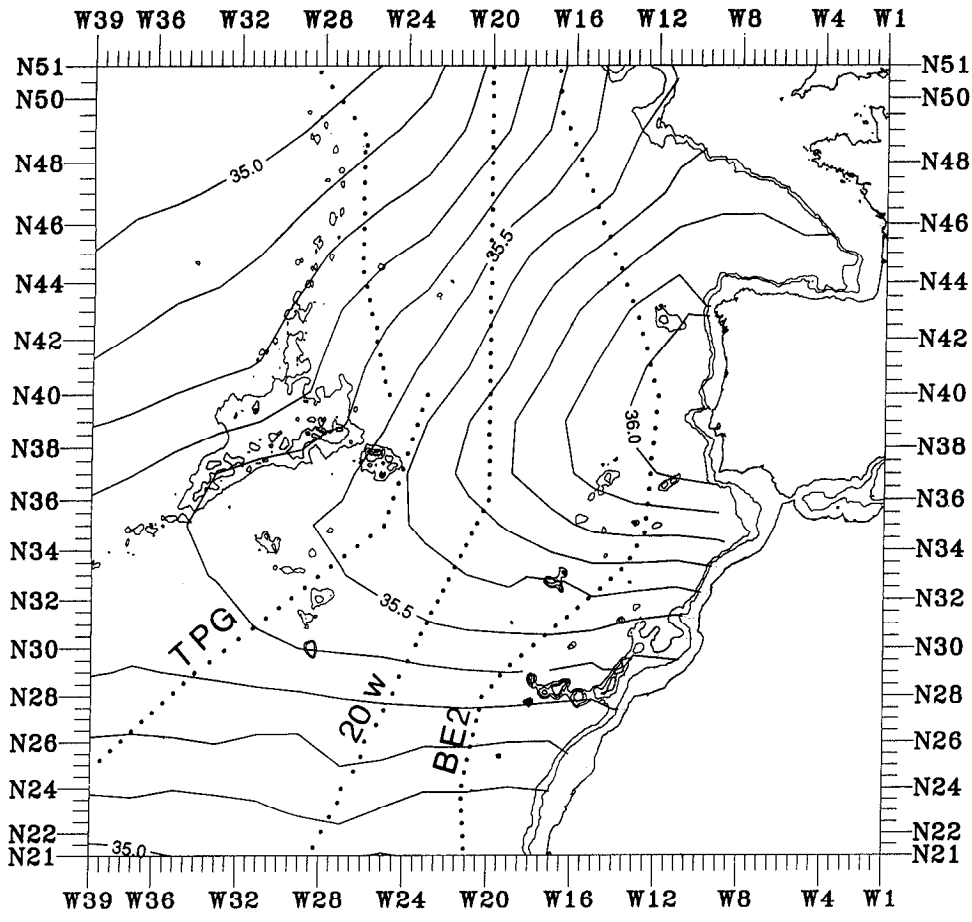

Figure 1. Distribution of the mean salinity field at 1000 db from Maillard (1986) (computer contouring from that author's original files), and the tracks of hydrographic lines TPG, 20W and BE2. Bathymetric contours 1000 m and 2000 m are shown.

nean salt (Section 4). (ii) The transition to the Subarctic Intermediate Water (SAIW) in the north, associated with quite different mesoscale processes (Section 5). (iii) In the north also but at a deeper level, the transition to the Labrador Sea Water (LSW, Section 6).

2. Cross-sections of the large-scale intrusion of Mediterranean Water

The large-scale intrusion of MW in the North-Atlantic Ocean stands out on the map of salinity at 1000 db reproduced in Figure 1 from Maillard (1986). The region situated west of the Iberian Peninsula between 37N and 43N shows the highest values and may be regarded as the "source" of MW for the ocean interior. Farther offshore the salinity signal is ridge-shaped with a crest line oriented in the west-

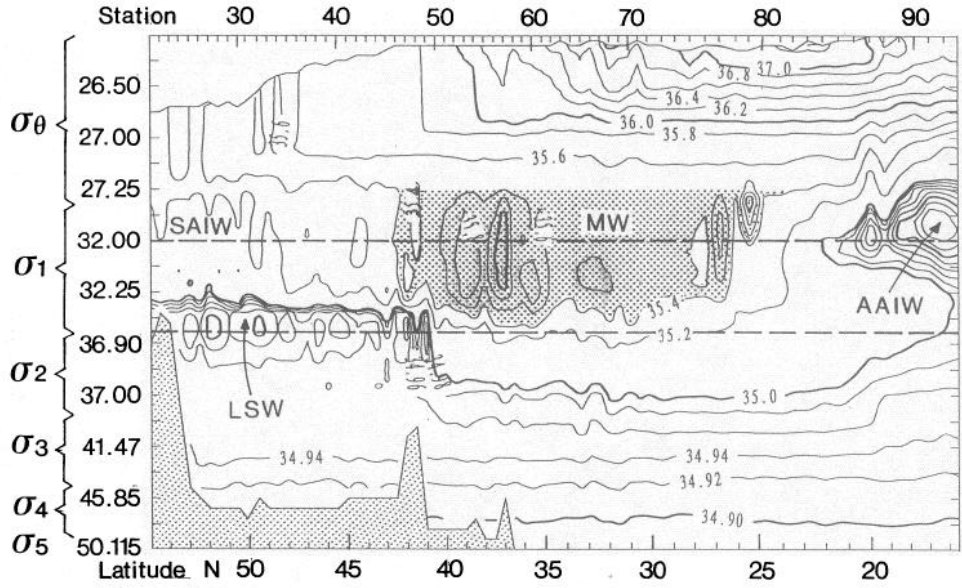

Figure 2. Vertical distribution of salinity along 20W, with respect to potential density. On the vertical scale the graduation is linear within each subdomain associated with a particular reference pressure, but different from one subdomain to another. Acronyms show the Mediterranean Water (MW) and the adjacent water masses: Subarctic Intermediate Water (SAIW), Antarctic Intermediate Water (AAIW), and Labrador Sea Water (LSW). Shading of the region ($S > 35.4$, $\sigma_\theta > 27.25$) helps visualize the Mediterranean Water.

southwest direction from $\simeq$ 38N at 12W to $\simeq$ 35N at 34W. The salinity decreases southward and northwestward on either side of the crest. Superposed on the salinity fields are the tracks of three hydrographic sections across the intrusion which provide well resolved meridional distributions of the MW.

The westernmost line is a composite one built from two cruises carried out in August and September 1983 in the framework of the TOPOGULF project (Topogulf Group, 1986). The imperfect union at 40N between the northern and southern parts carried out respectively from Research Vessels *Poseidon* and *Le Suroit,* is of no consequence for the purposes of the present study. That line is named TPG in the following. The central line named 20W and carried out in July and August 1988 during cruise *Oceanus* 202 is described in Tsuchiya *et al.* (1992). The eastern one was realized in May and June of that same year from the Research Vessel Jean Charcot. Its data are reported in Arhan *et al.* (1991) and, being part of the *BORD-EST* 2 cruise, it is here named BE2.

In Figure 2 we chose the line 20W to illustrate the meridional arrangement of water masses in the eastern basin. Density is used as the vertical coordinate in the displayed salinity section, so that any slope of the isohalines is indicative of an isopycnic variation of the thermohaline properties and may be interpreted as a water

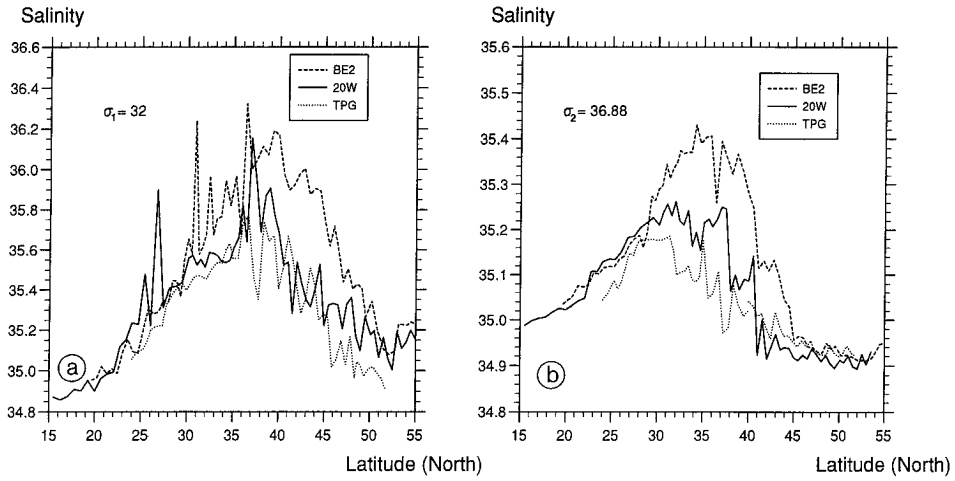

Figure 3. Salinity distribution along the three quasi-meridional lines (a) on the isopycnal σ_1 = 32.0, (b) on the isopycnal σ_2 = 36.88.

mass transition. The high salinity signal associated with the MW stands out, bordered in the north by fresher waters ($35.0 < S < 35.2$) containing a percentage of SAIW (Arhan, 1990; Read and Ellett, 1991), and in the south by salinities as low as 34.88 signaling an influence of AAIW. This figure shows the isopycnal $\sigma_1 = 32.0$ situated at the average pressure $p = 900$ db, which happens to intersect the cores of the three water masses and is therefore suitable for the study of their lateral diffusion. South of 41N the Mediterranean signal is seen in Figure 2 to extend downward to densities as high as $\sigma_2 \simeq 37.0$. North of that latitude the situation is different with a low salinity anomaly present there in the density range $32.35 < \sigma_{1,2} < 36.95$. This is the LSW known to be present in the eastern basin at these latitudes (Pingree, 1973; Talley and McCartney, 1982). The transition to deep MW takes the form of a sharp thermohaline front at 41N and, as the isopycnal $\sigma_2 = 36.88$ is here seen going through the core of LSW and the sharp front, it is this isopycnal, of average pressure 1800 db, that we choose in the following to illustrate the deep lateral gradient.

Figure 3 shows the salinity variations on the two isopycnals along the lines BE2, 20W and TPG. We focus here on the sloping portions of these curves, rather than their maxima, and point out below a few characteristic features of these domains.

On the southern side of the curves at $\sigma_1 = 32.0$ (Fig. 3a), the transition is characterized by an average salinity decrease of $\simeq 0.06$ per degree of latitude, a little more intense on BE2 north of 30N than on the two other curves. Superposed on this mean gradient on the BE2 and 20W lines are several positive salinity anomalies present at isolated stations and as high as 0.6, which are associated with meddies encountered along the cruise tracks. The meddies' signatures are of various intensities, probably because they are at different distances from their sites of formation

and because they may not have been sampled at their center where the anomaly is highest. As previous observations of meddies (Richardson *et al.,* 1989) have shown that they move with a southward velocity component, they can account for the southward diffusive salinity transport associated with the large-scale gradient of that parameter. This is what we assume in the following section, where the meddies' salt content, their southward propagation velocity and frequency of passage are the key parameters that determine the associated salt transport.

In the region of transition to SAIW north of the salinity maximum at $\sigma_1 = 32.0$ (Fig. 3a) the mean salinity gradient is roughly equivalent in intensity to that of the southern side, with again a slight difference between the BE2 curve and the two others. The superposed mesoscale signal is however very different in nature from that associated with the meddies. Instead of intense solitons, it takes here the form of a quasi-periodic signal with a crest-to-trough amplitude of about 0.3 and a typical wavelength of two degrees of latitude. This thermohaline variability is less spectacular and has been less studied than the one of the meddies, yet two experimental studies help to describe the mechanism.

In a region centered at 47N, 15W, a thermocline-intensified eddy was observed by Le Groupe Tourbillon (1983) to entrain northward and deform a patch of MW initially to the south of it, whose salinity anomaly of about 0.2 is comparable to the one observed here. Although Arhan and Colin de Verdière (1985) showed the MW bubble to have a weak associated dynamical signature, its behavior was mostly that of a tracer being stirred and mixed from above by the Tourbillon eddy. This is a situation very different from that prevailing on the southern side of the intrusion where MW is conveyed southward in coherent mesoscale vortices.

The other experiment, by Kupferman *et al.* (1986), reveals another type of north-south asymmetry. In the south there is no trace of parcels of AAIW being advected northward (Fig. 3a), the whole southward salinity transport being seemingly accounted for by the meddies. Conversely, SAIW which is normally found adjacent to the subpolar front at about 51N seems able to shed eddies toward the south. The above authors indeed found (near 48N, 21W) a tongue of SAIW some 250 km long and 60 km wide, pointing to the southeast, and still attached to the mother water. The associated salinity anomaly of about -0.2 is also comparable to the variability at the same latitude on the 20W curve in Figure 3a. At variance with the MW bubble entrained by the Tourbillon eddy, the SAIW tongue has a pronounced dynamical signature with typical velocities of order 0.2 m s^{-1}, and Kupferman *et al.* (1986) depict it as the eastern basin counterpart of the coherent cold core eddies known to detach from the Gulf Stream in the western basin.

Also on the northern side of the intrusion but at the density $\sigma_2 = 36.88$ (Fig. 3b), the transition with the LSW is again of a different pattern, at least along the BE2 and 20W lines. There the salinity gradient is dominated by two sharp fronts situated at $\simeq$44N and $\simeq$40N on BE2 and $\simeq$40N and $\simeq$37N on 20W. Mesoscale anomalies

present north of the 40N front at 20W are probably indicative of eddies being pinched off at the front. Such structures were indeed observed farther in the north by Schauer (1989) in a local hydrographic survey, and by Colin de Verdière *et al.* (1989) in Eulerian velocity and temperature time series. Schauer showed the structures to be cyclonic and characterized by a narrowing of isopycnals at their centers, and Colin de Verdière *et al.* named them "empty coherent vortices" as their cores are devoid of LSW although they are moving in a region and at depths where this water mass is normally present. As they are able to carry northward the waters of Mediterranean influence, we consider them in Section 6 below to be the mesoscale mixing agents of the MW at this depth.

3. A simple model of lateral mixing of the Mediterranean Water

The model uses a simple parameterization of the mixing of mesoscale structures and its large-scale consequences. It is limited to mixing balances and devoid of any dynamical ingredient. It is presented here, and used in the following section, in a configuration appropriate to the study of meddies. It is then adapted in Sections 5 and 6 to the processes at work in the regions of transition with SAIW and LSW.

Figure 4 (a, b) shows the model notation. The mesoscale structures are represented by cylinders of diameter $l/2$ moving southward along trajectories separated from each other by a distance d. Two successive meddies following the same trajectory are themselves separated by λ. We suppose that the meddies form at $y = 0$, and vanish through lateral diffusion at $y = -L$. They move at a bulk velocity v, which is also the exact velocity of their center point. The circular velocities affecting the other particles of the cylinders do not matter to the present study. In the water surrounding the cylinders non-vanishing velocities (U, V) are expected to satisfy the large-scale mass and salt budgets. The salinity $S(y, t)$ is decomposed into $S(y, t) = S_b(y) + \tilde{S}(y, t)$, where $S_b(y)$ is the background salinity and $\tilde{S}$ the mesoscale anomaly, positive in the meddies and equal to zero elsewhere. $S_M(y_c(t))$ and $\tilde{S}_M = S_M - S_b$ are the highest salinity and salinity anomaly encountered at a meddy center of latitude $y_c(t)$. Lateral diffusion coefficients K_M and K_L characterize the diffusive fluxes at the mesoscale and the large scale. Vertical diffusion is ignored.

The diffusion equation applied to salinity at a meddy center may be written as

$$\frac{dS_M}{dt} = K_M\left(\frac{\partial^2 S}{\partial x^2} + \frac{\partial^2 S}{\partial y^2}\right)\bigg|_{y=y_c},$$

or

$$\frac{dS_b}{dt} + \frac{d\tilde{S}_M}{dt} = K_M\left(\frac{\partial^2 S_b}{\partial x^2} + \frac{\partial^2 S_b}{\partial y^2}\right)\bigg|_{y=y_c} + K_M\left(\frac{\partial^2 \tilde{S}}{\partial x^2} + \frac{\partial^2 \tilde{S}}{\partial y^2}\right)\bigg|_{y=y_c}. \tag{1}$$

The second derivative $\partial^2 S_b/\partial x^2$ at the r.h.s. of this equation is equal to zero because S_b is a function of latitude only. The companion term $\partial^2 S_b/\partial y^2$ is itself two orders of

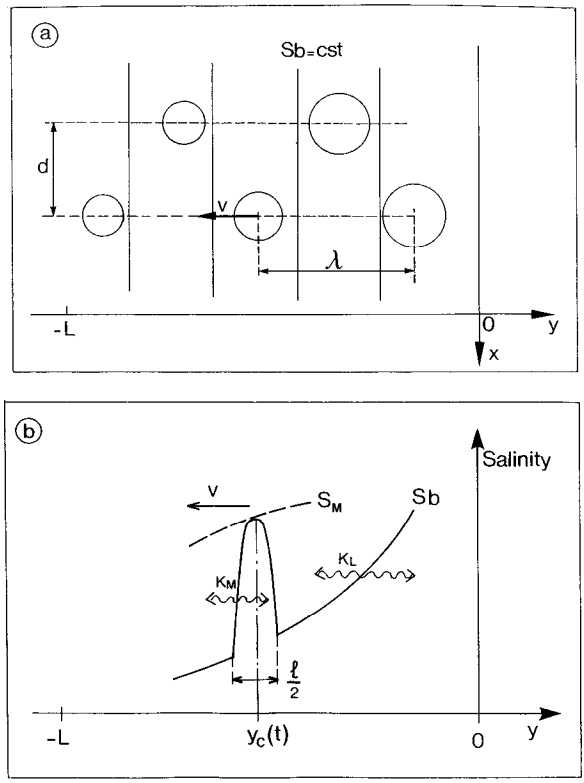

Figure 4. Notation for the mixing model. (a) Top view of a series of meddies moving along two neighboring trajectories. Coordinates x and y are positive eastward and northward. L is a (positive) distance, and v the algebraic velocity of the mesoscale structures. (b) Salinity notation in the vertical plane of the motion.

magnitude weaker than $\partial^2\tilde{S}/\partial y^2$, because S_b and $\tilde{S}$ show comparable variations (see Fig. 3) over length scales of order 1000 km for S_b, and 100 km for $\tilde{S}$. It is likewise eliminated. If we express the material derivatives following a particle as latitudinal variations, and make use of the meddy isotropy in the diffusive term, Eq. (1) becomes

$$\frac{d\tilde{S}_M}{dy} = -\frac{dS_b}{dy} + \frac{2K_M}{v}\frac{\partial^2\tilde{S}}{\partial y^2}\bigg|_{y=y_c}. \tag{2}$$

Eq. (2) states that, when a meddy moves southward, its associated anomaly tends to increase because of the decrease of $S_b(y)$, and decrease because of mixing.

The shape of the structure, $\tilde{S}(x,y)$, is needed to go further and evaluate the diffusive term on the r.h.s. of (2). Were salinity a passive tracer, application of the diffusion equation over the meddy domain would provide a solution for $\tilde{S}(x,y)$. But salinity is a dynamically active tracer, and the shape of the structure is subject to

strong dynamical constraints which we here ignore. We therefore choose to use a pre-specified shape, which we assume cosinusoïdal, and define a meddy by $\tilde{S} = \tilde{S}_M \cos(2\pi r/l)$ over the disc of radius $l/4$ centered at $y_c(t)$, where r is the distance to the eddy center. The usual name of "wavelength" is given to the size parameter l in the following although there is strictly no wavelength, of course, associated with the solitons thus defined. Using this formulation in the diffusive term of (2) leads to

$$\frac{d\tilde{S}_M}{dy} = -\frac{dS_b}{dy} - \frac{8\pi^2 K_M}{vl^2}\tilde{S}_M. \tag{3}$$

The salt content Q of a meddy is defined as the integral of salinity over the circular area of non-vanishing $\tilde{S}$:

$$Q = \int_o^{2\pi}\int_o^{l/4}\left(S_b + \tilde{S}_M \cos\frac{2\pi r}{l}\right) r\, dr\, d\theta,$$

or

$$Q = \frac{\pi l^2 S_b}{16} + \frac{(\pi/2 - 1)l^2\,\tilde{S}_M}{2\pi} \tag{4}$$

As a location which a meddy has just gone through is immediately re-occupied by background water, the salt transport associated with the meddy motion is only accounted for by the salt content anomaly $\tilde{Q} = (\pi/2 - 1)l^2\,\tilde{S}_M/2\pi$. As this quantity applies to an ocean strip of width d and successive meddies are separated by a distance λ, the salt flux across a given point is

$$F = \tilde{Q}v/\lambda d,$$

or

$$F = \left(\frac{\pi}{2} - 1\right) l^2\, v\, \tilde{S}_M/2\pi\lambda d \tag{5}$$

Equating this to the usual large-scale parameterization $F = -K_L dS_b/dy$ leads to

$$\frac{dS_b}{dy} = -\frac{\left(\frac{\pi}{2} - 1\right)l^2 v}{2\pi\lambda d K_L}\tilde{S}_M, \tag{6}$$

and substituting that expression for dS_b/dy in (3) provides the following new form of that equation:

$$\frac{d\tilde{S}_M}{dy} = \left[\frac{\left(\frac{\pi}{2} - 1\right)l^2 v}{2\pi\lambda d K_L} - \frac{8\pi^2 K_M}{vl^2}\right]\tilde{S}_M. \tag{7}$$

The model integrates Eqs. (6) and (7) from $y = 0$ to $y = -L$, given the boundary conditions $S_b(0)$, $\tilde{S}_M(0)$, and dS_b/dy at $y = 0$, of which the latter is adjusted in order to have the model salinity match the observed salinity at $y = -L$. Of the parameters ν, K_M, K_L, l, λ and d, some are specified at the outset from previous studies and others deduced from the observed salinity anomalies and background salinity gradient. The detailed adjustment procedures are described below for each application. Parameters ν, K_M, and K_L are assumed to be space-independent. So is λ in the first application. The wavelength l varies along the trajectory and is subject to certain constraints that we now discuss.

Neighborhood of $y = 0$: We assume that the anomaly separates from the background at $y = 0$, so that $\tilde{S}_M(0) = 0$ and

$$\frac{d\tilde{S}_M}{dy} \sim \frac{\tilde{S}_M}{y} \tag{8}$$

in the vicinity of this source point. As $d\tilde{S}_M/dy$ is necessarily negative for $\tilde{S}_M$ to increase at the early stages of the meddy life, the slope effect term $-dS_b/dy$ must be dominant in (7) so that

$$\frac{d\tilde{S}_M}{dy} \sim \frac{\left(\frac{\pi}{2} - 1\right) l^2 \nu}{2\pi\lambda d K_L} \tilde{S}_M \tag{9}$$

as the meddy detaches from the background. Combining (8) and (9) and assuming that the separation d between two neighboring trajectories equals $l(y)$ near $y = 0$, the wavelength is found to behave like

$$l_n(y) = \frac{2\pi\lambda K_L}{\left(\frac{\pi}{2} - 1\right)\nu y} \tag{10}$$

in the vicinity of that limit, which means that the structure originates with an infinite wavelength.

Neighborhood of $y = -L$: The same analysis may be done in the vicinity of $y = -L$ where the meddy is assumed to vanish. There we have

$$\frac{d\tilde{S}_M}{dy} \sim \frac{\tilde{S}_M}{y + L}, \tag{11}$$

and since the diffusion term is now dominant in (7):

$$\frac{d\tilde{S}_M}{dy} \sim -\frac{8\pi^2 K_M}{\nu l^2} \tilde{S}_M. \tag{12}$$

Combining (11) and (12) shows that $l(y)$ must vanish like

$$l_s(y) = 2\pi(-2K_M/v)^{1/2}(y + L)^{1/2} \tag{13}$$

in the last stages of the meddy life.

Definition of a "neutral" length l_o: The long distances covered by meddies before their decay have often been pointed out in the literature. Such a behavior occurs if $d\tilde{S}_M/dy$ is for some reason weak or vanishing over a significant part of the trajectory, i.e. if the diffusive and slope effect terms at the right-hand side of (3) or (7) cancel each other. Eq. (3) shows that a structure of intensity $\tilde{S}_M$ moving at a velocity v over a background gradient dS_b/dy will show no relative decrease if its size is

$$l_o = \left[(8\pi^2 K_M \tilde{S}_M)\Big/\left(-v\,\frac{dS_b}{dy}\right)\right]^{1/2}. \tag{14}$$

We name l_o the neutral wavelength. The same condition is expressed from (7) by

$$\frac{l_o^4}{\lambda d} = \frac{16\pi^3 K_L K_M}{\left(\frac{\pi}{2} - 1\right)v^2}. \tag{15}$$

Eqs. (14) and (15) are used in the next sections in the procedure of adjustment to observations. Depending on whether the other parameters present in (15) are assumed constant or not, the neutral wavelength may itself be constant or latitude dependent. As the lateral dimension of the structures in the model decreases from infinity at $y = 0$ (Eq. 10) to zero at $y = -L$ (Eq. 13), there is necessarily a latitude, or latitude range, where it equals the neutral wavelength.

4. The southern flank of the intrusion of Mediterranean Water

a. Mean trajectories of meddies. Following the discussion of the preceding sections we exclusively ascribe to the meddies the downgradient salt transport on the southern side of the intrusion. We consider a circular domain of diameter $D = O$ (100 km) in this region and suppose that successive meddies conveying salt contents $\tilde{Q}_i$ go through it at velocities $\mathbf{V}_i$. We name $\overline{\tilde{Q}_i}$ and $\overline{\mathbf{V}_i}$ the averaged values of $\tilde{Q}_i$ and $\mathbf{V}_i$ over a great number of passages. If T is the mean time lag between two successive meddies, an estimate of the mean salt flux across that diameter of the domain which is normal to $\overline{\mathbf{V}_i}$ is given by $\mathbf{F} = \overline{\tilde{Q}_i \mathbf{V}_i}/TD$. Further assuming that the fluctuations of $\tilde{Q}_i$ and $\mathbf{V}_i$ around their mean values are uncorrelated, the flux estimate becomes $\mathbf{F} = \overline{\tilde{Q}_i}\,\overline{\mathbf{V}_i}/TD$. Equating this to the large scale parameterization $\boldsymbol{F} = -K_L\,\nabla S$, we find that the mean trajectories thus defined are everywhere orthogonal to the isohalines.

Figure 5 shows a few of these trajectories drawn by hand across Maillard's (1986) salinity field at 1000 m. Also reported are the crest line of the salinity distribution,

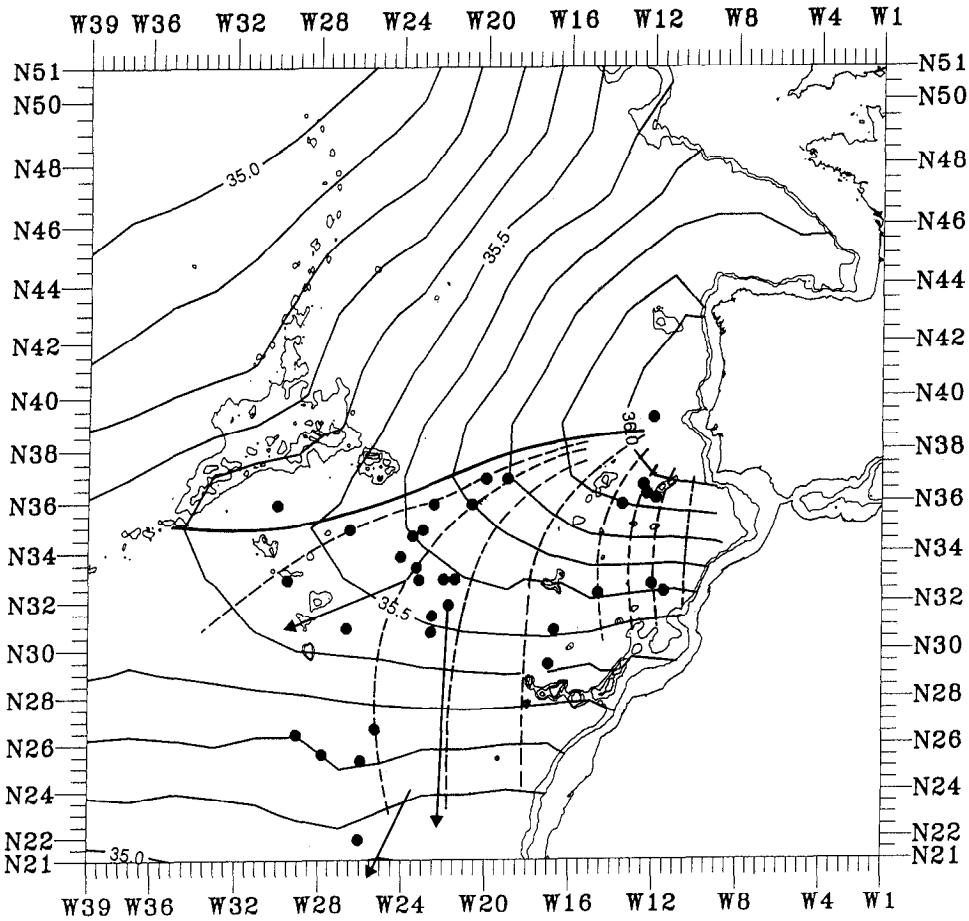

Figure 5. Positions of meddy sightings reported in the literature on Maillard's (1986) salinity distribution at 1000 m. Meddy observations are those reported in Richardson *et al.* (1991, Table 2) augmented by those of Table 1 of the present paper. Also superposed on the figure are: (i) The crest line of the large-scale salinity distribution (bold line). (ii) Expected mean meddy trajectories orthogonal to the isohalines. (iii) The mean displacement vectors of three meddies (Richardson *et al.*, 1989).

the positions of meddy sightings reported in the literature, and the mean displacement vectors of three individual meddies tracked with SOFAR floats (Richardson *et al.*, 1989). The meddy sightings are those of a previous compilation by Richardson *et al.* (1991) augmented by seven more recent observations listed in Table 1. It is remarkable that all of them but two are situated south of the crest line. Although the sampling was certainly not uniform, the observations appear to be gathered in two groups: East of 18W, a first group is likely to have originated in the south of the source region around 37N, 12W. Three meddies were indeed found there west of the

Table 1. Recent meddy observations added to the previous compilation by Richardson *et al.* (1991) and displayed in Figure 5.

Meddy Position		
Latitude °N	Longitude °W	Reference
22°	26°04	Zenk *et al.* (1991)
36°25	12°20	Arhan *et al.* (1994)
32°26	14°39	Arhan *et al.* (1994)
30°55	16°45	Arhan *et al.* (1994)
34°45	23°30	Pingree and Le Cann (1993a)
36°45	12°30	Pingree and Le Cann (1993b)
39°18	12°	Ollitrault (pers. comm., 1993)

Gorringe Bank at a location which Daniault *et al.* (1994) suggest to be a southern exit of the MW present in the Tagus Basin. From the displayed trajectories we should expect these meddies to end their lives against the continental slopes of Africa or of the Canary Archipelago. The second group found principally west of 22W has trajectories which originate in the immediate vicinity of the salinity crest line east of the Azores. These trajectories are nearly zonal and parallel to the crest line in their eastern part, and diverge while turning southwestward farther offshore. The meddies from this group should be expected to travel over longer distances.

Although we should not expect the individual paths to match the mean trajectories, the coincidence is remarkable for one of the reported displacement vectors. The two others cross the trajectories at angles around 35 degrees, yet illustrate the divergence of the meddies' routes in their region.

b. Model fit to the BE2 data. The tracks of cruises BE2 and 20W along which meddies were observed naturally do not follow trajectories, yet cut the background isohalines at high angles (Fig. 1). Fitting the model to these lines can therefore be considered an acceptable first approximation, to represent the growth and decay of meddies. We furthermore take advantage of the isohalines being mostly zonal, so that the meddies should move southward, and we measure the distances meridionally, instead of along the cruise tracks, in the following adjustments.

We consider that part of the BE2 salinity curve (Fig. 3a) comprised between 38N at about the crest line of the large-scale intrusion, and 20N at the southern end of the cruise track. We do not assume that meddies form at the former position, but rather at the Portuguese continental slope some 200 km in the east. At the other end we observe that the gradient of the background salinity nearly vanishes at 20N so that this must be, from Eq. (6), the latitude where meddies disappear on BE2. On the whole, we assume the meddies to travel over 2200 km in the neighborhood of BE2, a distance which includes the $\simeq 200$ km interval from the continental slope to the BE2 track, and the 2000 km long meridional journey from 38N to 20N. This provides the

range of the horizontal coordinate in Figure 6 illustrating the model fit. The broken line on this figure is the observed function $S(y)$. The adjustment is performed below so as to correctly reproduce the large-scale variation of the background salinity, and determine the history (in terms of $S_M(y)$) of the meddy observed at 32N.

We take some of the parameter values required in (6) and (7) from the two-year long meddy observation at about 22W reported by Richardson *et al.* (1989), Armi *et al.* (1989) and Hebert *et al.* (1990): we suppose that the structures move southward at a velocity $v = 1.8\ 10^{-2}$ m s^{-1} and that their properties mix with a diffusivity $K_M = 5$ m^2 s^{-1}. We further assume, according to the other studies quoted in the introduction, that the large-scale exchanges are characterized by $K_L = 500$ m^2 s^{-1}. We supposed, when deriving relation (10), that the distance d between two neighboring trajectories was equal to $l(y)$ in the vicinity of $y = 0$. We cannot, however, keep d identical to the wavelength over the whole trajectory because, as $l(y)$ vanishes at $y = -L$, that would amount to infinitely increase the number of meddies per unit of ocean width. To avoid that effect, d was kept equal to the neutral wavelength l_o south of the latitude where that dimension was encountered. Another typical distance could have been chosen, admittedly, but the l_o value quoted below provides a correct order of magnitude.

The separation λ between successive meddies of the same trajectory being assumed constant, this parameter and the function $l(y)$ are then determined by observing on the experimental curve of Figure 6 that the rate of variation of S_b is nearly constant in the central part of the trajectory. This is an indication, from (6), that the anomaly $\tilde{S}_M$ is itself quasi-constant, or that $l(y) \simeq l_o$. Replacing in (14) $\tilde{S}_M$ and dS_b/dy by their observed values 0.6 and $0.7\ 10^{-6}$ m^{-1} then gives $l_o = 140$ km, or a meddy radius $l_o/4$ of 35 km, a value quite suited to that kind of structure. Substituting this and the other parameter estimates in (15) then gives $\lambda \simeq 400$ km.

We saw in the preceding section that the wavelength must behave like $l_n(y)$ and $l_s(y)$ at the northern and southern ends of the trajectory. As the two functions were found to equal l_o at $y = -874$ km and $y = -1307$ km, respectively, the observed stable large-scale gradient dS_b/dy was reproduced by setting $l(y) = l_o$ over that interval, so that a composite function $l(y)$ could be defined as:

$$\begin{cases} l(y) = l_n(y) & \text{for } -874 \text{ km} < y < 0 \\ l(y) = l_o & \text{for } -1307 \text{ km} < y < -874 \text{ km} \\ l(y) = l_s(y) & \text{for } -2200 \text{ km} < y < -1307 \text{ km} \end{cases}$$

That function is displayed on Figure 6.

Eqs. (6) and (7) were integrated southward from $y = 0$ where the value $S_M(0) = S_b(0)$ was supposed to be 36.4, the maximum salinity along the continental slope south of the Tagus Plateau, and the derivative dS_b/dy was adjusted so as to reach a value $S_b \simeq 35.0$ at $y = -2200$ km. The resulting function $S_b(y)$ displayed on Figure 6 is a relatively good fit of the BE2 background salinity, and the $S_M(y)$ curve shows

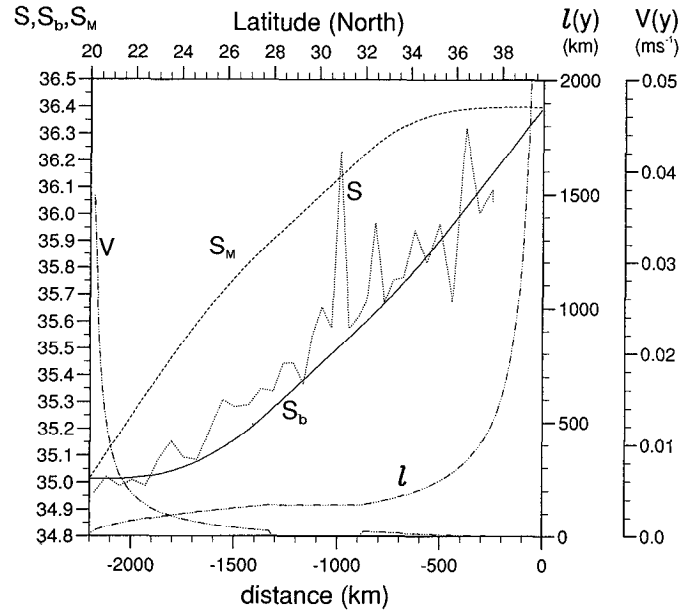

Figure 6. Result of the model fit to the BE2 data, described in Section 4 of the text. S is the salinity at $\sigma_1 = 32.0$ along the BE2 line. Model parameters S_b, S_M, l, and V are respectively: the adjusted background and maximum meddy salinities, the anomaly wavelength, and the meridional velocity required to balance the diffusive salinity transport in a one-dimensional advection-diffusion balance.

what could be the evolution of the meddy observed during the cruise at $y \simeq -1000$ km. Given the severe simplifications of the model, such as the neglect of vertical diffusion and the pre-specified and constant shape of the structure, the reconstructed evolution of the salinity anomaly is probably only a rough approximation of reality, yet provides a basis for a discussion of the successive phases of the meddy life.

The structure covers more than 500 km before it reaches its highest anomaly. That phase of growth results, in the model, from a stable maximum salinity S_M, itself a consequence of the large initial size of the eddy and the ensuing weak diffusion term in (1). The high wavelengths in the vicinity of the source appear unrealistic, yet their sharp decrease over the first four hundred kilometers could be an illustration of the detachment of meddies out of a larger pool of MW, perhaps through turbulent cascade. Daniault *et al.* (1994) indeed report large MW signals of diameters $\simeq 250$ km ($l \simeq 500$ km) in the West-Portugal region where the flow is highly variable (Käse *et al.*, 1989). Also, the meddy observed on BE2 at $\simeq 37$N or $\simeq 350$ km from the source point is predicted by the model to have a radius of $\simeq 75$ km, which is not unrealistic. The initial stability of S_M could also result, however, from real salinity distributions in the meddies which would be more rectangular (with vanishing

second derivative $\partial^2 S_M/\partial y^2$ at their center), than cosinusoïdal, as suggested by the observations of Hebert *et al.* (1990) and, to a lesser extent, by those of Armi and Zenk (1984). Such shapes would be compatible with a finite initial lateral dimension, and therefore may be more appropriate to the phase of growth of the meddies.

Once the model structure has attained its highest anomaly, it is noticeable that it keeps it over more than 1000 km. As seen above, that can only occur if the terms of diffusive decay and background salinity decrease at the r.h.s. of (2) balance each other. With the assumed shape of the structure that can also be expressed by saying that the lateral dimension remains close to the mixing neutral length defined by (14). As the size of the structure is determined by dynamical considerations here ignored, we can only note that apparent balance, but any attempt to explain it would of course require a study of the inner dynamics of the structure and their links to the mixing processes.

More than the details of the meddy evolution, what was expected from the model in the first place was a scaling relation between the mesoscale and large-scale diffusivities. That relation is provided by Eq. (15), valid over the central part of the trajectory. Though established on the simplified hypothesis described in Section 3, the link between the likely (and here prespecified) orders of magnitudes of K_L and K_M, given the velocity v of the structure, was shown to be compatible with a quite plausible set of dimension parameters, l, d and λ.

The meddy decays rapidly (0.55 in salinity over 500 km) in the last part of its trajectory. At these stages the parabolic shrinking of the structure is determined by the increasing importance of the diffusive term in Eq. (7). That rapid decay is here a diagnostic result of the model fit without any indication, of course, of the mixing processes which may cause it.

The vanishing lateral gradient of the background salinity is another characteristic of the decay region. That characteristic is a direct consequence of the hypothesis that meddies are the exclusive contributors to the large-scale salinity flux. Were this true, the geographical distribution of salinity on an adequate isopycnic surface would readily provide the outer limit of the domain where meddies can be found. That hypothesis should not, however, be considered as rigorously exact: a recent analysis of Lagrangian trajectories at the MW level by Spall *et al.* (1993) suggests that mixing at the MW depths in the Canary Basin is also contributed to by other forms of low-frequency variability characterized by either quasi-zonal motions or wave-like oscillations.

Although this study is not aimed at discussing the large-scale advection-diffusion balance, we computed for this example the meridional velocity V of the background water required to balance the meddies salt transport. Again we take advantage of the isohalines being quasi-zonal so that the derivatives dS_b/dx and d^2S_b/dx^2 vanish, and V may be estimated as $V = K_L(d^2S_b/dy^2)/(dS_b/dy)$. V is northward everywhere on

Figure 6 (except in the central segment where l was set equal to l_o), but only significant near the southern end of the trajectories where it reaches values around $3\ 10^{-2}$ m s^{-1}. Horizontal non-divergence would there require background zonal velocities such that $dU/dx > 0$, a gradient consistent with Stramma's (1984) and Zenk *et al.'s* (1991) observations of a westward flow reaching such depths at about 20N, in that region which the latter authors call the Cape Verde Frontal Zone.

c. Model fit to the 20W data and to the meddy observed by Armi et al. (1989). Along 20W the meridional gradient of the background salinity vanishes at $\simeq$15N (Fig. 3b) which is also the latitude where the meddies must disappear. Taking again $y = 0$ at 38N we now have $L = 2500$ km. The salinity is plotted over that distance range on Figure 7. As in the preceding fit we use $v = -1.8\ 10^{-2}$ m s^{-1}, $K_M = 5$ m^2 s^{-1} and $K_L = 500$ m^2 s^{-1}.

The salinity curve along 20W differs from that along BE2 (Fig. 6) by negative second derivatives d^2S_b/dy^2 north of $\simeq$25N, associated with a weak meridional gradient between 30N and 35N. That lower gradient, which corresponds on Maillard's (1986) map to a change of direction of the isohalines, implies there a weaker southward component of the diffusive flux. In terms of meddy motions, it should most certainly be related to the meddies moving in a dominant westward direction on the immediate south of the crest line (Fig. 5), and more toward the south at lower latitudes. This is reproduced in the model by using a latitude-dependent λ parameter: we assume that meddies coming from the east may, by a change of direction, rejoin our pseudo-trajectory north of 25N and thus increase the meddy density along the line, and decrease λ. Latitude 38N is therefore no longer the "source point" of all the meddies travelling along the trajectory, and we do not extend the fit of the model to that latitude. We no longer need the function $l_n(y)$ and consider that $l(y)$ equals $l_s(y)$ over the latitudinal range of the adjustment.

Although a meddy observed at $\simeq$27N along 20W (Fig. 7) could have provided the $\tilde{S}_M$ value required for the model fitting, we found it preferable to use the parameters of the meddy observed by Armi *et al.* (1989) and Hebert *et al.* (1990) whose path, shown as the easternmost arrow on Figure 5, happens to be in the vicinity of 20W. As the structure was first observed at 32N we chose that latitude as the northern limit of the adjustment, and assumed the distance between two neighboring meddy trajectories to be constant and equal to the wavelength at that latitude, i.e. $d = l_s$ (32N) = 200 km. The parameters of the meddy at the times of its four surveys are reported in Table 2 and displayed in Figure 7. The background salinities from Hebert *et al.* (1990) match those of the 20W line and show the same tendency of a weaker meridional gradient around 30N. The maximum salinity anomalies in the meddy are between 0.63 and 0.82 and do not show any decrease from 32W to 22N. The size of the structure being specified at the outset, a non-varying $\tilde{S}_M$ is here obtained, from

Table 2. Parameters of the meddy reported by Armi *et al.* (1989) and Hebert *et al.* (1990) at the times of the four CTD surveys spanning a two-year period. The salinities at $\sigma_1 = 32.0$ are estimated from Figure 3 of Hebert *et al.* and the wavelength l is four times the "total radius" reported in Figure 16 of Armi *et al.*

Latitude (°N)	y (km)	S_b	S_M	$\tilde{S}_M$	l (km)
32°	−667	35.60	36.23	0.63	232
28°20	−1075	35.50	36.23	0.73	156
26°40	−1259	35.35	36.17	0.82	140
22°	−1778	35.05	35.70	0.65	120

Eq. (15), by a variable λ related to $l(y)$ by:

$$\lambda(y) = \left(\frac{\pi}{2} - 1\right) v^2 l^4(y)/(16\pi^3 d K_L K_M). \tag{16}$$

We satisfy both requirements of a larger λ north of ≃25N and a quasi-vanishing $d\tilde{S}_M/dy$ from 32N to 22N by using relation (16) between 32N and 25N (Fig. 7). That causes the average distance between successive meddies to decrease from ≃1200 km to ≃400 km, and the value at 25N is kept south of that latitude. The model fit to

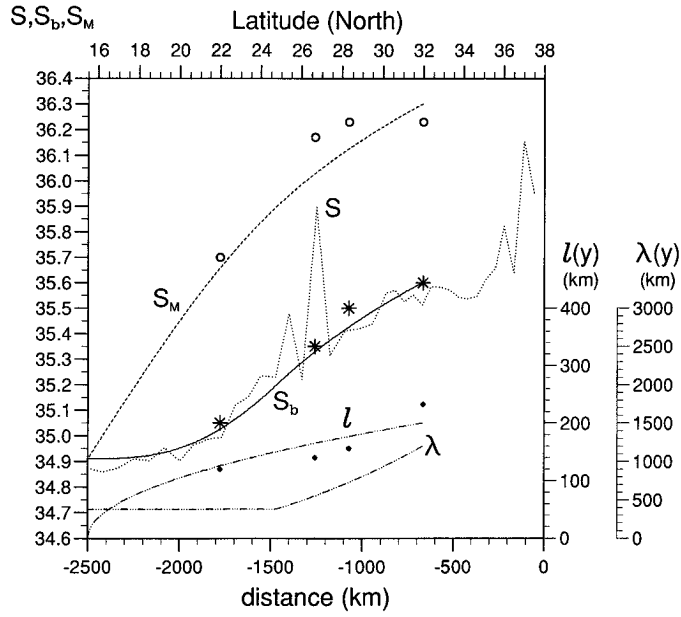

Figure 7. Result of the model fit to the 20W data and the meddy observed by Armi *et al.* (1989), described in Section 4 of the text. Notations S, S_M, S_b and l are as in Figure 6. Parameter λ is the average distance between two successive meddies along the pseudo-trajectory. Values of S_b, S_M and l for the meddy observed by Armi *et al.* (1989) and Hebert *et al.* (1990) are also shown.

reality is again satisfactory with the meddy keeping its highest salinity anomaly $\tilde{S}_M \simeq 0.6$ for more than 1100 km, then decaying over the last 700 km.

The above model adjustment, like the fit to the BE2 data, rests on the existence of a significant fraction of the trajectory over which the rate of decrease of S_M is equivalent to that of S_b. Having assumed that the structure is only eroded by horizontal diffusion, this balance is expressed by Eq. (15) which is satisfied again with quite realistic values of the parameters l, d, and λ. For this meddy, however, Hebert *et al.* (1990) suggest that the salinity decrease was due to vertical mixing until the double-diffusive intrusions present at the rim of the structure reached the center. The question then raises whether salinity erosion by vertical diffusion, instead of horizontal diffusion, could balance the background salinity decrease.

With vertical mixing, Eq. (2) transforms into

$$\frac{d\bar{S}_M}{dy} = -\frac{dS_b}{dy} + \frac{K_v}{v}\frac{\partial^2 \bar{S}}{\partial z^2}\bigg|_{y=y_c}, \tag{17}$$

where K_v is the vertical diffusivity, and the term $\partial^2 S_b/\partial z^2$ has been neglected. An approximate value of the second derivative is $-5\ 10^{-6}\ \mathrm{m}^{-2}$, from the salinity profiles reported in Armi *et al.* (1989). With the observed values $dS_b/dy \simeq 0.7\ 10^{-6}\ \mathrm{m}^{-1}$ and $v \simeq -2\ 10^{-2}\ \mathrm{m\ s}^{-1}$, a diffusivity $K_v \simeq 2\ 10^{-3}\ \mathrm{m}^2\ \mathrm{s}^{-1}$ would be required for the anomaly to be stable. That being a value probably too high by one order of magnitude, it is unlikely that vertical mixing can equilibrate the background salinity decrease. A more classical value $K_v = O(10^{-4}\mathrm{m}^2\ \mathrm{s}^{-1})$ would, on the other hand, be consistent with the constant maximum salinity S_M observed between 32N and 28N, and support Hebert *et al.'s* (1990) scenario, with vertical diffusion—and Eq. (17)—prevailing north of the latter latitude, and horizontal diffusion—and Eq. (2)—taking over south of it. Although Eq. (15) would only be valid south of 28N, the model fit presented above would not be significantly altered south of that latitude.

5. Transition with the Subarctic Intermediate Water

a. A pronounced thermohaline mesoscale variability. We use data from the following four additional cruises to describe the high thermohaline variability of the region (Fig. 8):

- A zonal transect across the eastern basin at 41N, carried out in 1977 during *Discovery* cruise 81, and described in Saunders (1980). We name that line 41N.
- A similar transect along 48N (named 48N in the following), carried out during cruise C.S.S. *Hudson* 82-002, and reported in Hendry (1989).
- Two repetitions of segment IJ of line 20W from cruises *Discovery* 181 (Read *et al.,* 1991) and *Discovery* 189 (King *et al.,* 1991). These two cruises (which we refer to as D181 and D189) have extensions along segment JL of the 41N line.

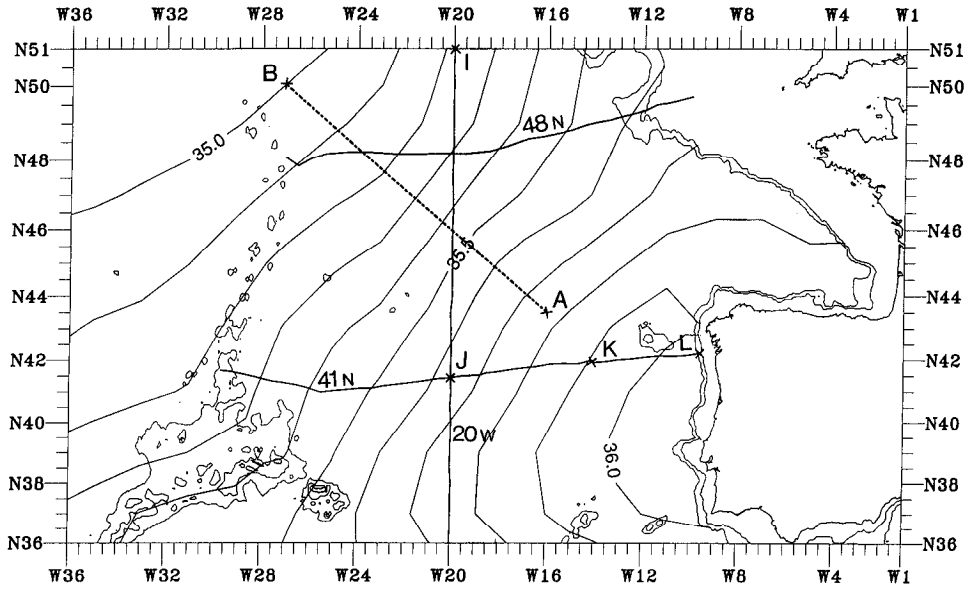

Figure 8. Salinity distribution at 1000 m from Maillard (1986) on the northern side of the large-scale intrusion of MW, with the 1000 m and 2000 m bathymetric contours. Also reported are: —the tracks of cruises 20W, 41N, 48N, and two segments (LJ and JI) of cruises D181 and D189; —the pseudo-trajectory AB orthogonal to the isohalines, used for the model fit in Section 5.

Figure 9 shows the vertical distribution of salinity along 48N. Shading the area characterized by $\{S < 35.2, p < 1000 \text{ db}\}$ illustrates the alternation of fresher and saltier waters influenced respectively by SAIW and MW. The SAIW character is dominant at the western end of the section while a core of MW is seen against the continental slope in the east. The variability also stands out on the curves of salinity at $\sigma_1 = 32.0$ along 20W and the two zonal lines 41N and 48N (Fig. 10a, b). The two realizations D181 and D189 along 20W confirm the salinity mesoscale variability to have a crest-to-crest amplitude between 0.4 and 0.2, decreasing northward. The amplitude is similar along 48N but lower than 0.2 along 41N.

At the large scale the mean salinity gradients are comparable on the meridional and zonal lines (Fig. 10a, b), in accordance with the $\simeq 45$ degrees inclination of the isohalines with respect to the parallels on Maillard's (1986) map (Fig. 8). The net diffusive salt transport must therefore be oriented northwestward, and we expect it to result from mesoscale saline anomalies moving on the average in that direction and fresher ones in the opposite direction. We fit the model below to such a pseudo-trajectory shown by the segment AB on Figure 8. As we have no salinity data along that line, we assume the main characteristics of the variability observed along 20W to be valid also along that segment.

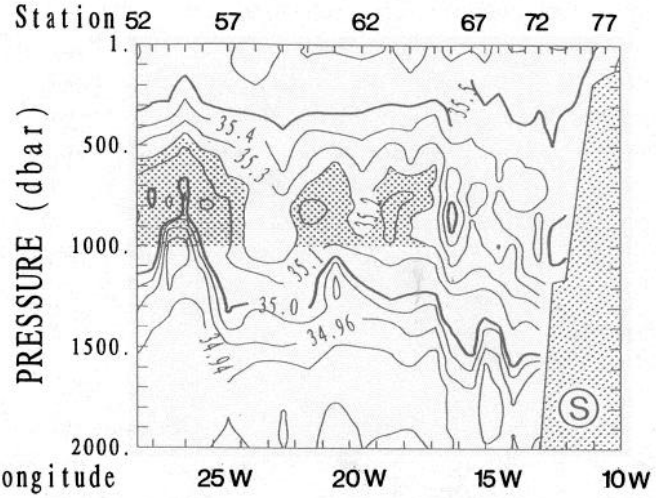

Figure 9. Vertical distribution of salinity along 48N, illustrating the pronounced thermohaline variability in the transition region between MW and SAIW. The domain ($S < 35.2$, $p < 1000$ db) is shaded for a better visualization of the SAIW influence.

b. A model version for opposite motions of opposite anomalies. The experimental results of Le Groupe Tourbillon (1983) and Kupferman *et al.* (1986) quoted above in Section 2 suggest the mesoscale mixing mechanisms between SAIW and MW to be multiple and complex. Whereas the SAIW bubbles detached from the North-

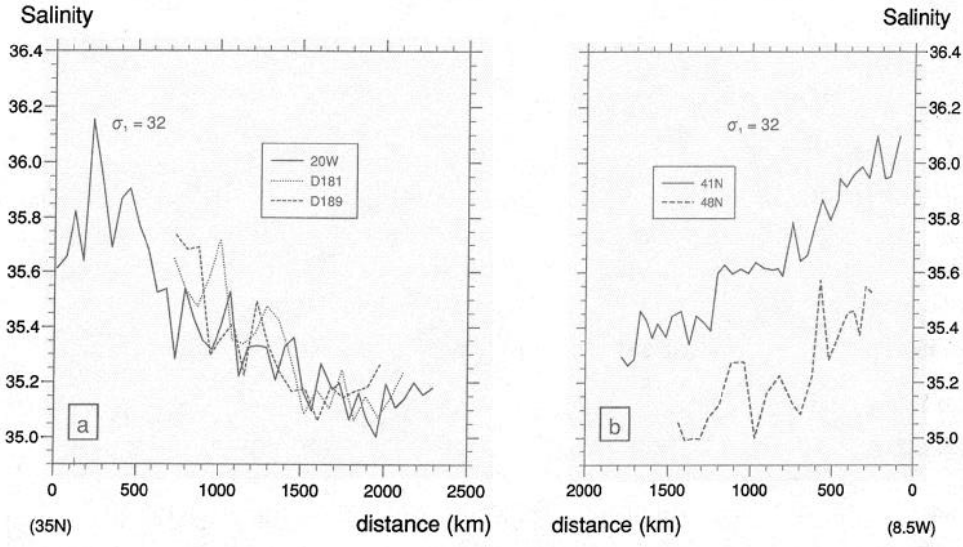

Figure 10. Illustration of the salinity variability at $\sigma_1 = 32.0$ on the northern flank of the MW intrusion from: (a) the three realizations 20W, D181, D189 along the meridional line 20W, (b) the two zonal transects 41N and 48N.

Atlantic Current seem to behave like coherent structures, the MW parcels would be expected to deform and perhaps break up under the effect of the thermocline-intensified mesoscale turbulence. Applying our simplified mixing model to such structures seems a bold exercise, yet Figure 10a suggests the tracer "streakiness" (Garrett, 1983) to be less developed than could be inferred from the sole Tourbillon experiment. Typical wavelengths between 200 km and 300 km do exist throughout the transition region, particularly along 20W and D181, an indication that the MW patches are able to keep their initial coherence, probably owing to their weak associated dynamical signal. This gives more confidence that the model may be appropriate to a certain extent, and we use it below in a configuration where opposite salinity anomalies move in opposite directions along the pseudo-trajectory AB (Fig. 8).

We assume that the positive anomalies $\tilde{S}_{M1}$ go from A to B at the velocity v and the negative ones $\tilde{S}_{M2}$ from B to A at the velocity $-v$. Successive structures of the same type, and neighboring trajectories, are separated by the wavelengths l_1 or l_2. The salt transports associated with the MW and SAIW structures combine into the total salt transport, so that the same reasoning which led to (6) now gives

$$\frac{dS_b}{dy} = -\frac{\left(\frac{\pi}{2} - 1\right)v}{2\pi K_L}(\tilde{S}_{M1} - \tilde{S}_{M2}). \tag{18}$$

Writing Eq. (3) for each kind of anomaly and using (18) we also obtain:

$$\frac{d\tilde{S}_{M1}}{dy} = \frac{\left(\frac{\pi}{2} - 1\right)v}{2\pi K_L}(\tilde{S}_{M1} - \tilde{S}_{M2}) - \frac{8\pi^2 K_M}{vl_1^2}\tilde{S}_{M1} \tag{19}$$

and

$$\frac{d\tilde{S}_{M2}}{dy} = \frac{\left(\frac{\pi}{2} - 1\right)v}{2\pi K_L}(\tilde{S}_{M1} - \tilde{S}_{M2}) + \frac{8\pi^2 K_M}{vl_2^2}\tilde{S}_{M2} \tag{20}$$

Eqs. (18) to (20) govern the variations of S_b, $\tilde{S}_{M1}$, $\tilde{S}_{M2}$, given the other parameters.

c. The model fit. The segment AB (Fig. 8) has a length L = 1100 km and the coordinate y along it is taken to increase northwestward. The background salinity varies from 35.75 at A(y = 0) to 35.00 at B. We assume the intensity and wavelengths of the variability along AB to be similar to those observed along the segment JI of 20W and illustrated on Figure 10a. In particular we impose that $\tilde{S}_{M1}$ = 0.4 and $\tilde{S}_{M2}$ = 0 at y = 0 where we start the integration, and try to reproduce a crest-to-trough amplitude of $\simeq$0.15 at B as observed at I.

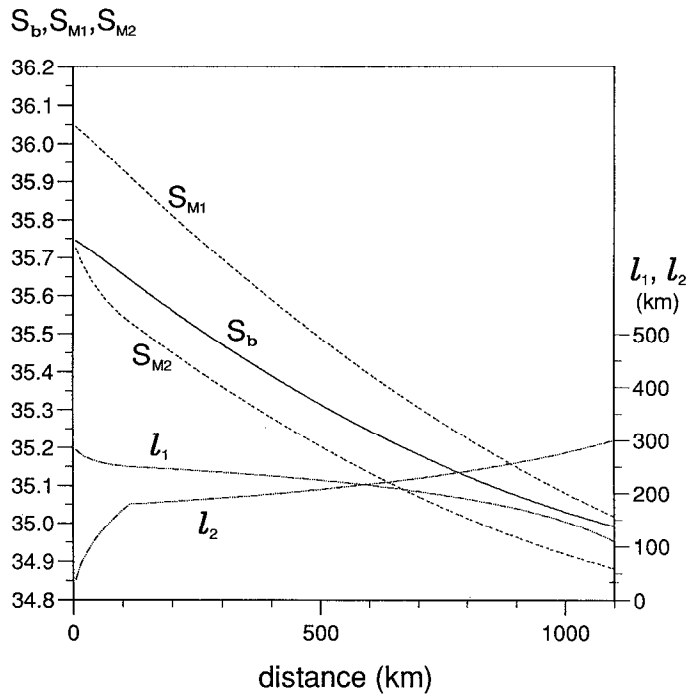

Figure 11. Result of the model fit along the pseudo-trajectory AB (Fig. 8) using variability parameters inferred from Figure 10a. S_b is the background salinity, S_{M1} and l_1 the maximum salinity and wavelength of the mesoscale MW parcels travelling from A to B, and S_{M2} and l_2 their homologues for the SAIW parcels travelling from B to A.

At $y \simeq L/2$ (Fig. 10a) we have $\tilde{S}_{M1} - \tilde{S}_{M2} \simeq 0.3$ and $dS_b/dy \simeq -0.75\ 10^{-6}\ \mathrm{m}^{-1}$ which from (18) gives $\nu/K_L = 27\ 10^{-6}\ \mathrm{m}^{-1}$. Taking the a priori estimate $K_L = 500\ \mathrm{m^2\ s^{-1}}$ we find $\nu = 1.4\ 10^{-2}\ \mathrm{m\ s^{-1}}$, which is a plausible result. In order to have $\tilde{S}_{M2}$ vanish at $y = 0$ we impose $l_2(y) = 2\pi(2K_M/\nu)^{1/2}\ y^{1/2}$ in the vicinity of that limit, following the same analysis which led to Eq. (13). The wavelengths are otherwise not pre-determined, but rather diagnosed from Eqs. (19) and (20) and the observed values of $d\tilde{S}_{M1}/dy$ and $d\tilde{S}_{M2}/dy$. From Figure 10a the crest-to-trough amplitude of the variability decreases northward at a rate $d(\tilde{S}_{M1} - \tilde{S}_{M2})/dy \simeq -0.25\ 10^{-6}\ \mathrm{m}^{-1}$, a figure which apparently should be ascribed more to $\tilde{S}_{M1}$ than to $\tilde{S}_{M2}$. We then stipulate that $d\tilde{S}_{M1}/dy = -0.25\ 10^{-6}\ \mathrm{m}^{-1}$ and $d\tilde{S}_{M2}/dy = 0$ and, given an *a priori* estimate of K_M, compute $l_1(y)$ and $l_2(y)$ from (19) and (20) at each step of integration.

The model fit is shown in Figure 11 for a choice of the mesoscale diffusivity $K_M = 50\ \mathrm{m^2\ s^{-1}}$. Such a high value was required for the wavelengths to be in the observed range between 200 km and 300 km. Although we forced $\tilde{S}_{M2}$ to vanish at $y = 0$ we did not try to model the birth and last stages of the MW and SAIW anomalies and merely regard Figure 11 as a scaling model. It shows that given the observed characteristics

of the variability and the large-scale salinity gradient, the anomalies must travel at a typical velocity $v \simeq 1.4\ 10^{-2}$ m s^{-1} and mix with a diffusivity $K_M \simeq 50$ m^2 s^{-1}, for the large-scale scale diffusivity to be $K_L = 500$ m^2 s^{-1}. We should remark however, from Eqs. (19) and (20), that other parameter values conserving the ratios v/K_L and v/K_M would not alter the salinity curves of Figure 11. As an example, the set of parameters $K_L = 10^3$ m^2 s^{-1}, $v = 2.8\ 10^{-2}$ m s^{-1} and $K_M = 100$ m^2 s^{-1} would similarly provide a good fit to reality. If the ratios v/K_L and v/K_M are conserved, so must be K_L/K_M, which rules out any possibility of having a K_M value as low as the one (5 m^2 s^{-1}) associated with the meddies, for that would imply a too low value of K_L around 50 m^2 s^{-1}. A larger K_M on the northern side of the MW intrusion therefore seems a robust result, reminiscent of the order of magnitude 100 m^2 s^{-1} proposed by Colin de Verdière *et al.* (1986) from the Tourbillon experiment. These authors regarded the salinity as a passive tracer and, following Rhines and Young (1983), considered such a value to be a shear-augmented diffusivity.

6. Transition to Labrador Sea Water

a. Evidence of eddy detachment at the front between deep MW and LSW. Figure 12 shows Maillard's (1986) salinity distribution at 1800 db, a pressure close to that of isopycnal $\sigma_2 = 36.88$ used on Figure 3b. Also shown are the tracks of the two cruises BE2 and 20W and the locations (noted F) of the northernmost front on each of them. The front line is close and almost parallel to the topographic ridge Azores-Biscay of average depth around 3000 m, a possible indication of a bathymetric influence on the mid-depth flow in this region.

We suggested in Section 2 that eddy detachment from that front could be responsible for the mixing between deep MW and LSW. The mechanism would therefore be analogous to the meddy production, with the difference that a pronounced thermohaline front not present in the south here marks the origin of the eddies, which are also deeper, cyclonic, and move northward. Schauer (1989) describes such a structure found at 47N, 20W. That position is shown in Figure 12 along with three other observations listed in the same study. We added two salinity anomalies higher than 0.05 present near the front along the 20W and D189 lines. One is visible at $\simeq$41N on the salinity section of Figure 2. The other one appears at 42N on Figure 13 showing salinity along the route KJI (Fig. 8) of D189. An additional one is even present at $\simeq$18W on the zonal part of the route, which apparently has just detached from the front marked by the quasi-vertical isohalines 34.98 and 35.00 at $\simeq$17W.

From the inclination of the isohalines on Figure 12 the eddies should move on the average toward the northwest. Having no hydrographic data along that direction, we again use the three realizations along 20W to adjust the model below.

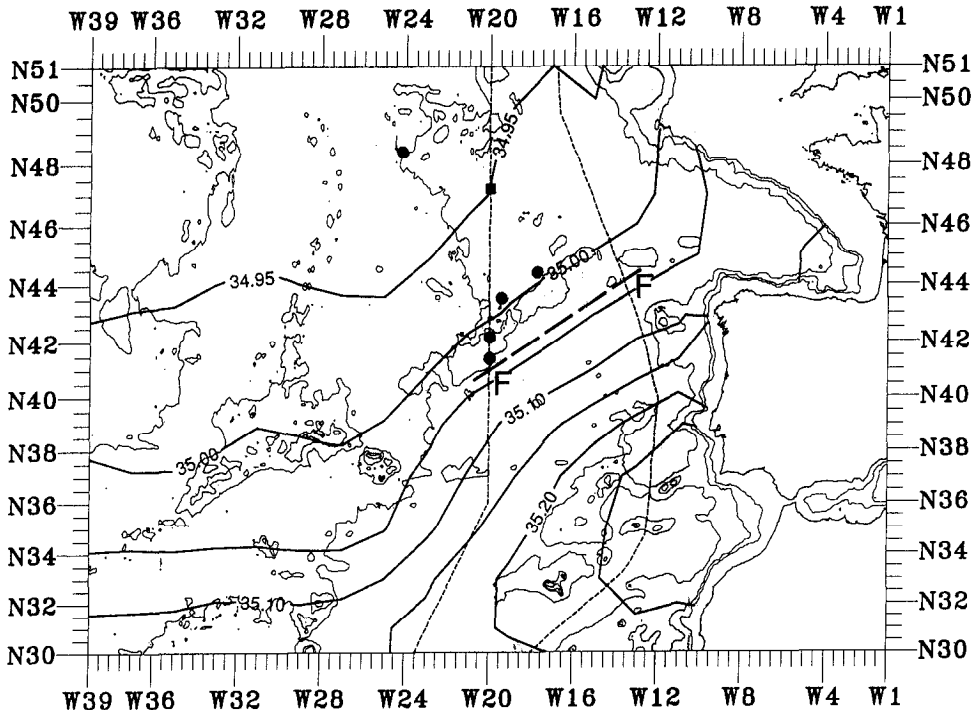

Figure 12. Salinity distribution at 1800 m from Maillard (1986), with the 1000 m, 2000 m and 4000 m bathymetric contours and the BE2 and 20W tracks. Line FF shows the thermohaline front separating the deep MW from the LSW. Also displayed are the positions of deep saline eddy sightings from Schauer (1989) augmented by two salinity anomalies higher than .05 on cruises 20W and D189. Out of them the black square at 20W, 47N marks the intensive survey of such an eddy in Schauer's paper.

b. Model representation of the decay of Schauer's (1989) eddy. In this application the model is again represented by Eqs. (6) and (7) with now a positive velocity v. We take $y = 0$ at 40N on Figure 14 showing the model fit. The salinity curves of cruises 20W, D181 and D189 show the front at $y \simeq 100$ km and a nearly vanishing large-scale salinity gradient at $y \simeq 1000$ km (or $\simeq$49N), the value we assign to L. The point representing Schauer's (1989) eddy is also shown at $y = 640$ km, $S_M = 35.0$. We chose to fit the model to that eddy rather than to those observed on 20W and D189 which were probably not sampled in their centers. The model proved unable to represent the radical change of slope of the background salinity at the edge of the front, so that we only start the integration at $y = 150$ km where the structure has just detached from the front. We then represent $l(y)$ by the equivalent of Eq. (13):

$$l(y) = 2\pi(2K_M/v)^{1/2}(L - y)^{1/2}. \tag{21}$$

Observing that $l \simeq 200$ km at $y = 150$ km, Eq. (21) gives $K_M/v \simeq 6\ 10^2$ m, which we

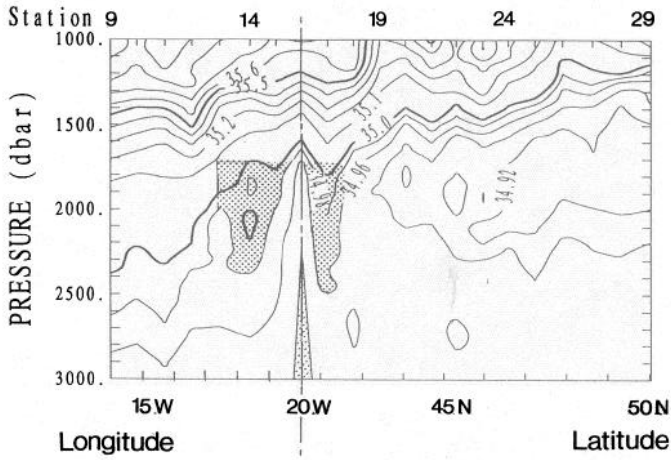

Figure 13. Salinity section along route *KJI* (Fig. 8), showing two saline eddies in the vicinity of the deep thermohaline front. The front appears as quasi-vertical isohalines 34.98 and 35.00 at ≃17W on the zonal part of the section, and shading identifies the two eddies. A bathymetric peak (from the Azores-Biscaye Ridge) as shallow as ≃2300 m shows up at point *J* at the junction of the zonal and meridional parts of the line.

satisfy by setting $K_M = 6\ m^2\ s^{-1}$ and $\nu = 10^{-2}\ m\ s^{-1}$. The K_M value comparable to the one used in Section 4 for the meddies is thought adequate for mixing at the rim of coherent vortices, while the ν estimate probably provides the correct order of magnitude. The experimental $S(y)$ curves on Figure 14 also provide a rough estimate of $dS_b/dy \simeq 10^{-7}\ m^{-1}$ at $y = 150$ km. We use this and a first guess of $\tilde{S}_M$ at the same latitude $y = 150$ km to estimate λ from Eq. (6). The distance between neighboring trajectories, also needed in that equation, is given the constant value $d = 200$ km of the wavelength as the structure detach from the front. Finally, the initial $\tilde{S}_M$ had to be adjusted to 0.15 for the $S_M(y)$ curve to meet the point of Schauer's eddy and the ensuing distance between two successive eddies is $\lambda = 550$ km.

The theoretical curves are displayed on Figure 14. Here again other parameter combinations could have led to the same salinity curves, but the ones retained here show the expected orders of magnitude. The adjustment is also satisfactory in other respects: the anomaly amplitude required near the front ($\tilde{S}_M = 0.15$) compares well with the salinity step at the front itself, and the wavelength curve predicts at the position of Schauer's (1989) eddy a diameter $l/2 \simeq 60$ km, similar to what is reported in that study.

In Section 4 we observed the meddy anomaly $\tilde{S}_M$ to first increase, then remain quasi-constant over long distances, an indication that the wavelength of the structure was close to the neutral wavelength required to equilibrate the diffusive and slope-effect terms on the right-hand side of Eq. (7). The neutral wavelength is here $l_o \simeq 240$ km. Dynamical considerations determine the scale of the eddies as they

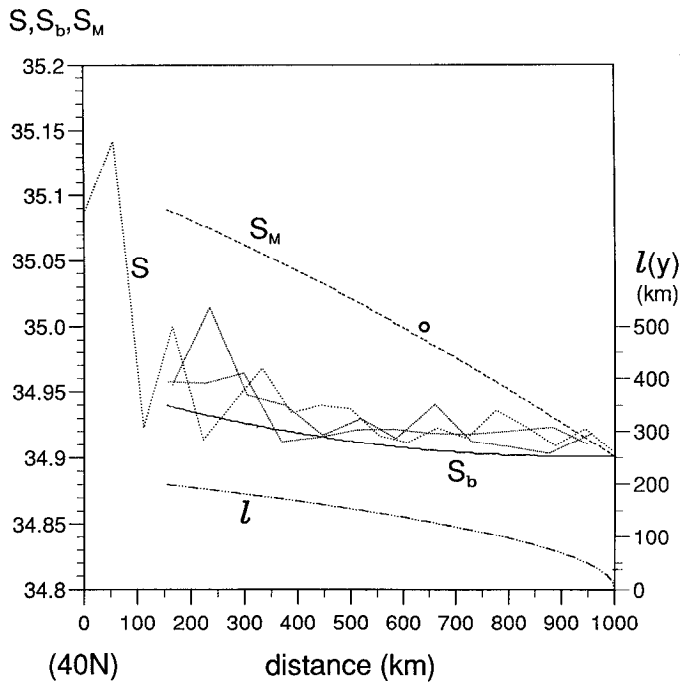

Figure 14. Result of the model fit to the LSW-deep MW transition region and Schauer's (1989) eddy. The experimental salinity distribution at $\sigma_2 = 36.88$ along 20W is shown by its three realizations 20W, D181, D189. An open circle marks the salinity in the core of Schauer's eddy. Notations are as in Figure 6.

detach from the front. Apparently it so happens here that that scale is smaller than l_o, so that diffusion rapidly dominates the r.h.s. of Eq. (7) and the structure decreases from its early stage on, as observed in Figure 14.

7. Summary and conclusions

The first result of this study is the illustration provided by three quasi-meridional hydrographic lines that the large-scale mixing of MW with its adjacent water masses occurs through different mesoscale processes. A simplified mixing model relating the mesoscale and large-scale diffusivities was used diagnostically to help analyze these differences and verify the compatibility of previous experimental estimates of the diffusivities.

Table 3 summarizes the parameter values used to adjust the model to the three studied lateral boundaries of the MW. Some of these parameters were specified from the meridional CTD lines or using results from previous studies, the others were provided by the model fit. The large-scale background salinity gradients at $\sigma_1 = 32.0$ are comparable on either side of the intrusion and, given similar diffusivities K_L,

Table 3. Summary of the mesoscale and large-scale parameters used to fit the unidirectional mixing model to the boundaries between MW and the three adjacent water masses.

Boundary		MW-AAIW		MW-SAIW	Deep MW-LSW
Fit to		BE2	20W + Armi *et al.*'s (1989) eddy	20W, D181 D189	20W, D181, D189 + Schauer's (1989) eddy
Mesoscale parameters	$\tilde{S}_M$	0.6	0.6	± 0.15	≤ 0.15
	$v(\mathrm{m\ s^{-1}})$	$-1.8\ 10^{-12}$	$-1.8\ 10^{-2}$	$1.4\ 10^{-2}$	10^{-2}
	$l(10^3\ \mathrm{m})$	140	160	$200 << 300$	150
	$d(10^3\ \mathrm{m})$	140	200	$200 << 300$	200
	$\lambda(10^3\ \mathrm{m})$	400	≥ 400	Periodic signal	550
	$K_M(\mathrm{m^2\ s^{-1}})$	5	5	50	6
Large-scale parameters	$L(10^3\ \mathrm{m})$	2200	2500	1100	1000
	$dS_b/dy(\mathrm{m^{-1}})$	$0.7\ 10^{-6}$	$0.7\ 10^{-6}$	$-0.75\ 10^{-6}$	Front
	$K_L(\mathrm{m^2\ s^{-1}})$	500	500	500	500

predict equivalent southward and northward salt fluxes. In the south the flux is accounted for by meddies of typical intensities $\tilde{S}_M = 0.6$ travelling at an average distance of $\simeq 400$ km from one another. On the northern side the same salinity flux results from opposite motions of series of MW and SAIW parcels of respective intensities $+0.15$ and -0.15, following each other at a distance of $\simeq 200$ km. The boundary with the LSW at $\sigma_2 = 36.88$ is characterized by a sharp thermohaline front oriented in a southwest-northeast direction between 40N and 45N. Eddies containing deep MW propagating northward after detachment from that front were shown to produce a salt transport consistent with the weak meridional background salinity gradient present there.

Large-scale diffusivities $K_L = 500\ \mathrm{m^2\ s^{-1}}$ were assumed to fit the model to the three transition regions. Other solutions could have been obtained in response to different K_L values, but the ones presented in Table 3 are thought to provide correct orders of magnitude. At the three boundaries the model shows how the mesoscale parameters l, v, and K_M, associated with quite plausible eddy separations, combine into the prescribed large-scale diffusivity.

The severe simplifications of the model (one-dimension, pre-specified shape of the mesoscale thermohaline anomalies, neglect of vertical mixing) should, however, be kept in mind when considering the details of the growth and decay of the mesoscale structures. Although one-dimension is not much of a handicap to study the evolution of coherent structures along their trajectories, the pre-specified shape and neglect of vertical mixing are certainly more questionable when applying the model to meddies. A rectangular (rather than cosinusoïdal) shape would have allowed finite lateral dimensions of the structures at their birth. Assuming that the meddy centers are only subject to (weak) vertical mixing until they are reached by the double-diffusive

intrusions active at the periphery of the lenses could have been another improvement. These are, however, meddy-specific characteristics which we did not retain, being concerned by the three water mass boundaries. The model based on solely lateral diffusion led us to introduce the "neutral wavelength" l_o for which the structure shows no relative decay. The ability of some meddies to live over several years could be related to these structures having dimensions close to l_o. The eddies which originate at the deep thermohaline front between LSW and deep MW apparently have smaller dimensions than their local neutral wavelength, hence a shorter life duration. Dynamical prediction of the initial wavelengths of the mesoscale structures would be useful for a better understanding of these differences.

The one-dimensional model is clearly still less appropriate to the study of mixing at the MW-SAIW boundary where two-dimensional mesoscale turbulence prevails. We nevertheless used it as a first approach to illustrate the combined effects of opposite salinity anomalies travelling on average in opposite directions. The high K_M value (~ 50 m^2 s^{-1}) found there seems a robust result consistent with previous experimental estimates. It could perhaps be explained by the tendency of the MW to behave there like a passive tracer, at variance with the other cases where it is conveyed in coherent vortices. Further dynamical studies using a more appropriate model would be required to find out to what extent the thermocline eddies or SAIW eddies present in the region are able to break down the initial coherence of the MW bubbles.

Acknowledgments. M. Arhan was supported for this study by the IFREMER Grant 210160 and contract 87-473 from the EPSHOM (Etablissement Principal du Service Hydrographique et Océanographique de la Marine). B. King was funded by a Fellowship in the Joint Environment Programme of National Power and PowerGen. The authors are grateful to A. Colin de Verdière for helpful discussions and to M. McCartney and R. Pollard for setting at their disposal the data from their cruises *Oceanus* 202 and *Discovery* 181, respectively. They are also thankful to C. Maillard for the use of her files of averaged salinity, and to C. Fontaine, J. Le Gall and J. Kervella for their contributions to the preparation of the manuscript.

REFERENCES

Arhan, M. 1990. The North Atlantic Current and Subarctic Intermediate Water. J. Mar. Res., *48,* 109–144.

Arhan, M., A. Billant, A. Colin de Verdière, L. Mémery and P. Tréguer. 1991. CTD-O_2 and nutrients along the eastern boundary of the North-Atlantic Ocean from 60N to 20N. Bord-Est Data Report, volume 1. Campagnes Océanographiques Françaises, no. 13, IFREMER, 115 pp.

Arhan, M. and A. Colin de Verdière. 1985. Dynamics of eddy motions in the eastern North-Atlantic. J. Phys. Oceanogr., *15,* 153–170.

Arhan, M., A. Colin de Verdière and L. Mémery. 1994. The eastern boundary of the subtropical North-Atlantic. J. Phys. Oceanogr., *24,* 1295–1316.

Armi, L, D. Hebert, N. Oakey, J. F. Price, P. L. Richardson, H. T. Rossby and B. Ruddick. 1989. Two years in the life of a Mediterranean salt lens. J. Phys. Oceanogr., *19,* 354–370.

Armi, L. and H. Stommel. 1983. Four views of a portion of the North Atlantic subtropical gyre. J. Phys. Oceanogr., *13,* 828–857.

Armi, L. and W. Zenk. 1984. Large lenses of highly saline Mediterranean Water. J. Phys. Oceanogr., *14,* 1560–1576.

Colin de Verdière, A., J. G. Harvey and M. Arhan. 1986. Stirring and mixing of thermohaline anomalies. J. Mar. Res., *44,* 93–118.

Colin de Verdière, A., H. Mercier and M. Arhan. 1989. Mesoscale variability transition from the western to the eastern Atlantic along 48N. J. Phys. Oceanogr., *19,* 1149–1170.

Daniault, N., J. P. Mazé and M. Arhan. 1994. Circulation and mixing of the Mediterranean Water west of the Iberian Peninsula. Deep-Sea Res., *41,* 1685–1714.

Garrett, C. 1983. On the initial streakiness of a dispersing tracer in two- and three-dimensional turbulence. Dyn. Atm. Ocean., *7,* 265–277.

Hebert, D., N. Oakey and B. Ruddick. 1990. Evolution of a Mediterranean salt lens: scalar properties. J. Phys. Oceanogr., *20,* 1468–1483.

Hendry, R. M. 1989. Hydrographic measurements from C.S.S. *Hudson* cruise 82-002. Canadian Technical Report of Hydrography and Ocean Sciences, *118,* 112 pp.

Hogg, N. G. 1987. A least-squares fit of the advective-diffusive equations to Levitus Atlas data. J. Mar. Res., *45,* 347–375.

Joyce, T. M. 1977. A note on the lateral mixing of water masses. J. Phys. Oceanogr., *7,* 626–629.

Käse, R. H., A. Beckmann and H. H. Hinrichsen, 1989. Observational evidence of salt lens formation in the Iberian Basin. J. Geophys. Res., *94,* C4, 4905–4912.

King, B. A., S. G. Alderson, S. Bacon, T. J. P. Gwilliam, C. Hirst, R. Paylor, J. F. Read and J. C. Swallow. 1991. CTDO station data from the North East Atlantic from RRS *Discovery* cruise 189. Report no. 287, Institute of Oceanographic Sciences, Deacon Laboratory, 182 pp.

Kupferman, S. L., G. A. Becker, W. F. Simmons, U. Schauer, M. G. Marietta and H. Nices. 1986. An intense cold core eddy in the North-East Atlantic. Nature, *319,* 474–477.

Le Groupe Tourbillon. 1983. The Tourbillon experiment: a study of a mesoscale eddy in the eastern North Atlantic. Deep-Sea Res., *30,* 475–511.

Maillard, C. 1986. Atlas hydrologique de l'Atlantique Nord-Est. Publications IFREMER. 133 plates.

Needler, G. T. and R. A. Heath. 1975. Diffusion coefficients calculated from the Mediterranean salinity anomaly in the North Atlantic Ocean. J. Phys. Oceanogr., *5,* 173–182.

Pingree, R. D. 1973. A component of Labrador Sea Water in the Bay of Biscay. Limnol. Oceanogr., *18,* 711–718.

Pingree, R. D. and B. Le Cann. 1993a. Structure of a Meddy (Bobby 92) southeast of the Azores. Deep-Sea Res., *40,* 2077–2103.

—— 1993b. A shallow Meddy (A Smeddy) from the secondary Mediterranean Salinity Maximum. J. Geophys. Res., *98,* C11, 20169–20185.

Read, J. F. and D. J. Ellett. 1991. Subarctic Intermediate Water in the eastern North-Atlantic. International Council for the Exploration of the Sea. C.M. 1991/C:42, Hydrography Committee.

Read, J. F., R. T. Pollard and C. Hirst. 1991. CTD data from the North-East Atlantic, April 1989, collected on RRS *Discovery* Cruise 181. Report Nb 285, Institute of Oceanographic Sciences, Deacon Laboratory, 157 pp.

Rhines, P. B. and R. W. Young. 1983. How rapidly is a passive scalar mixed within closed streamlines? J. Fluid Mech., *133,* 133–145.

Richardson, P. L., M. S. McCartney and C. Maillard. 1991. A search for meddies in historical data. Dyn. Atm. Ocean, *15,* 241–265.

Richardson, P. L. and K. Mooney. 1975. The Mediterranean outflow–A simple advection-diffusion model. J. Phys. Oceanogr., *5,* 476–482.

Richardson, P. L., D. Walsh, L. Armi, M. Schröder and J. F. Price. 1989. Tracking three meddies with SOFAR floats. J. Phys. Oceanogr., *19,* 371–383.

Saunders, P. M. 1980. CTD data obtained during *Discovery* cruise 81. Data Report no. 17, Institute of Oceanographic Sciences.

Schauer, U. 1989. A deep saline cyclonic eddy in the west European basin. Deep-Sea Res., *36,* 1549–1565.

Spall, M. A., P. L. Richardson and J. Price. 1993. Advection and eddy mixing in the Mediterranean salt tongue. J. Mar. Res., *51,* 797–818.

Stramma, L. 1984. Geostrophic transport in the warm water sphere of the eastern subtropical North Atlantic. J. Mar. Res., *42,* 537–558.

Talley, L. D. and M. S. McCartney. 1982. Distribution and circulation of Labrador Sea Water. J. Phys. Oceanogr., *12,* 1189–1205.

Topogulf Group. 1986. Data Report Volume 1: CTD, O_2 and nutrients. Ber. Institut für Meereskunde, Kiel, *154,* 183 pp.

Tsuchiya, M., L. D. Talley and M. S. McCartney. 1992. An eastern Atlantic section from Iceland southward across the equator. Deep-Sea Res., *39,* 1885–1917.

Zenk, W., B. Klein and M. Schröder. 1991. Cape Verde Frontal Zone. Deep-Sea Res., *38,* (Suppl. 1), S505–S530.

Received: *7 April, 1994;* Revised: *16 May 1995.*